Electronic Supplementary Information

Ni-Mo-O nanorod-derived composite catalysts for efficient alkaline water-to-hydrogen Conversion via urea electrolysis

Zi-You Yu[§], Chao-Chao Lang[§], Min-Rui Gao, Yu Chen, Qi-Qi Fu, Yu Duan, and Shu-Hong Yu**

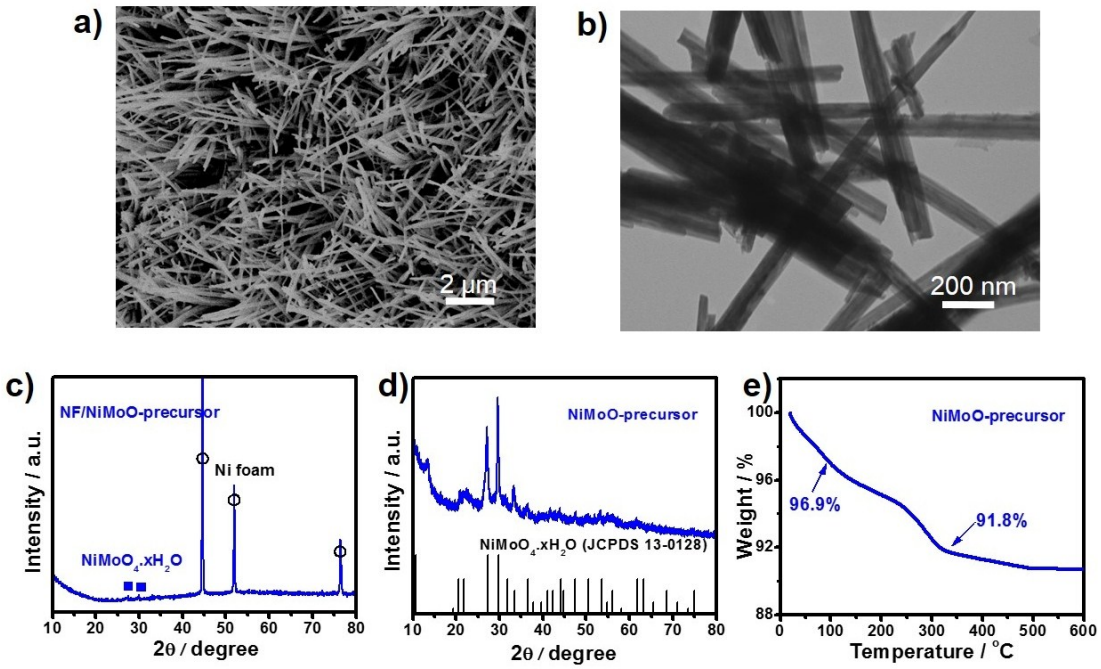

Fig. S1. Characterization of NF/NiMoO-precursor. a) SEM image of NF/NiMoO-precursor. b) TEM image of NiMoO-precursor nanorods. c) XRD pattern of NF/NiMoO-precursor. d) XRD pattern of NiMoO-precursor powder obtained by the ultrasound from NF/NiMoO-precursor. e) TG analysis curve of NiMoO-precursor in N_2 atmosphere. Due to the strong XRD pattern peaks from NF substrate, it is difficult to index the phase of active materials. Therefore, all XRD patterns were performed for the powder samples by the ultrasound from the 3D NF substrate.

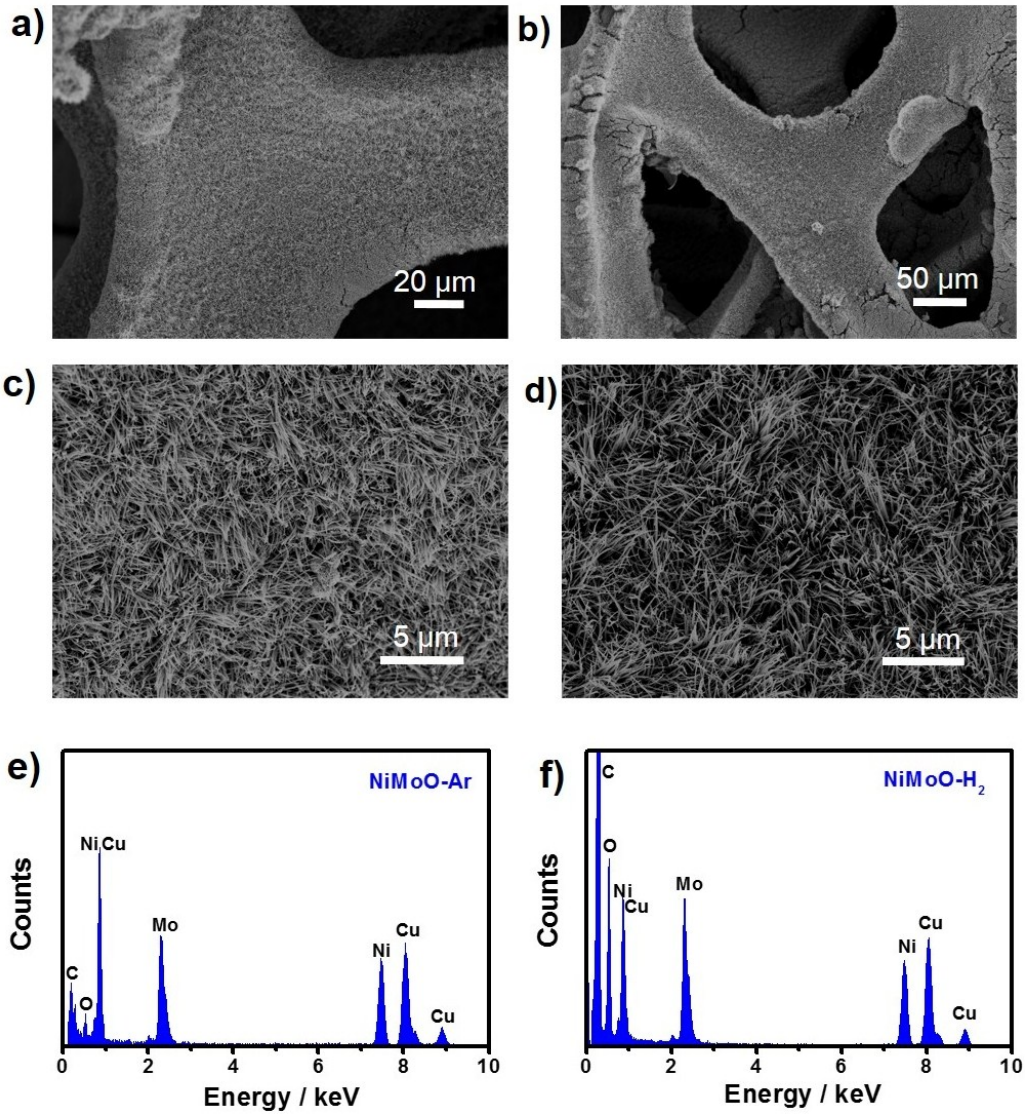

Fig. S2. Characterization of NF/NiMoO-Ar and NF/NiMoO-H_2. a,c) SEM images of NF/NiMoO-Ar. b,d) SEM images of NF/NiMoO-H_2. e) EDX spectrum of NiMoO-Ar. f) EDX spectrum of NiMoO-H_2. The signals of Cu and C elements in (e,f) come from the carbon-coated TEM grid.

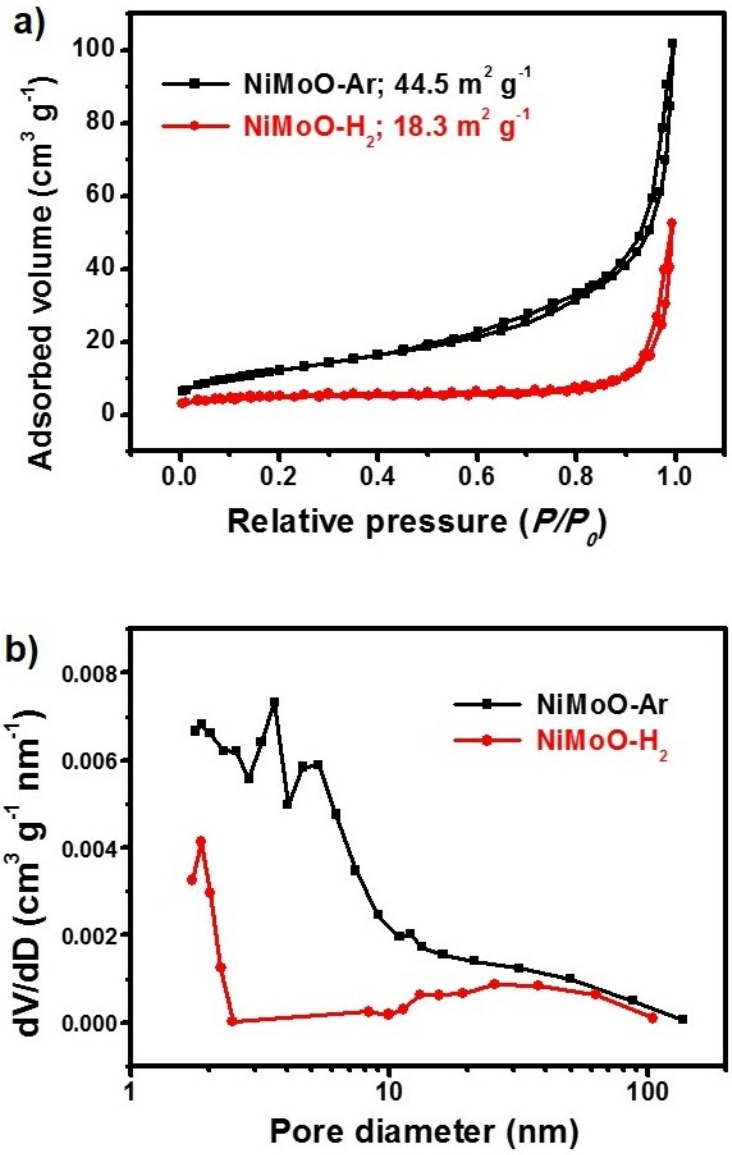

Fig. S3. a) Nitrogen adsorption-desorption isotherms of NiMoO-Ar and NiMoO-H_2. b) Pore size distribution of NiMoO-Ar and NiMoO-H_2.

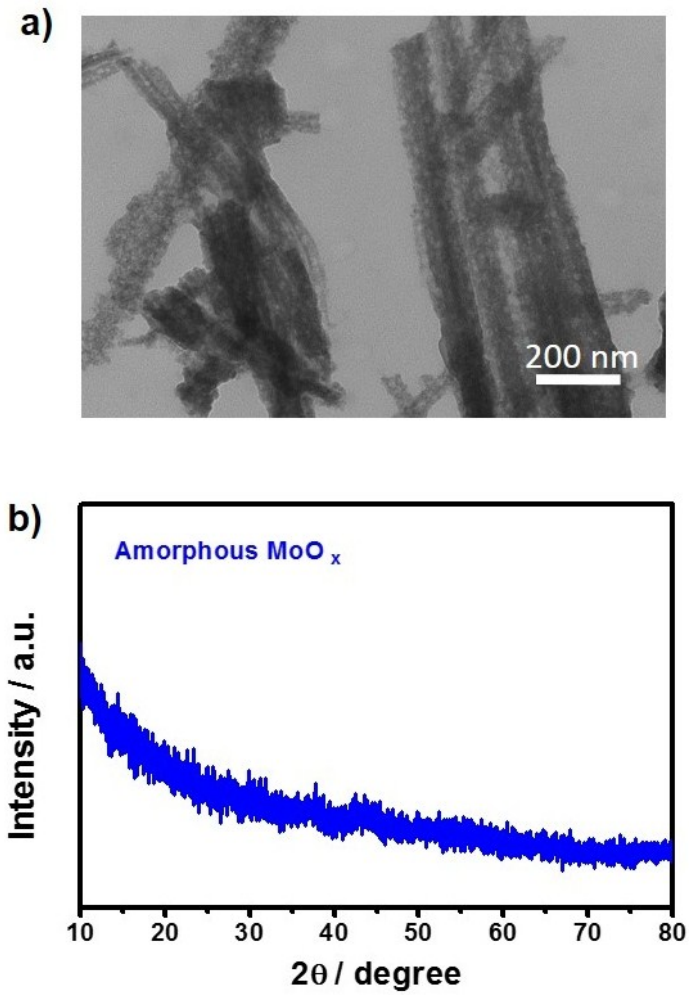

Fig. S4. Characterization of MoO_x. a) TEM image of MoO_x. b) XRD pattern of MoO_x. MoO_x was obtained by acid treatment of NiMoO-H_2 in 0.1 M HCl solution, showing the amorphous phase.

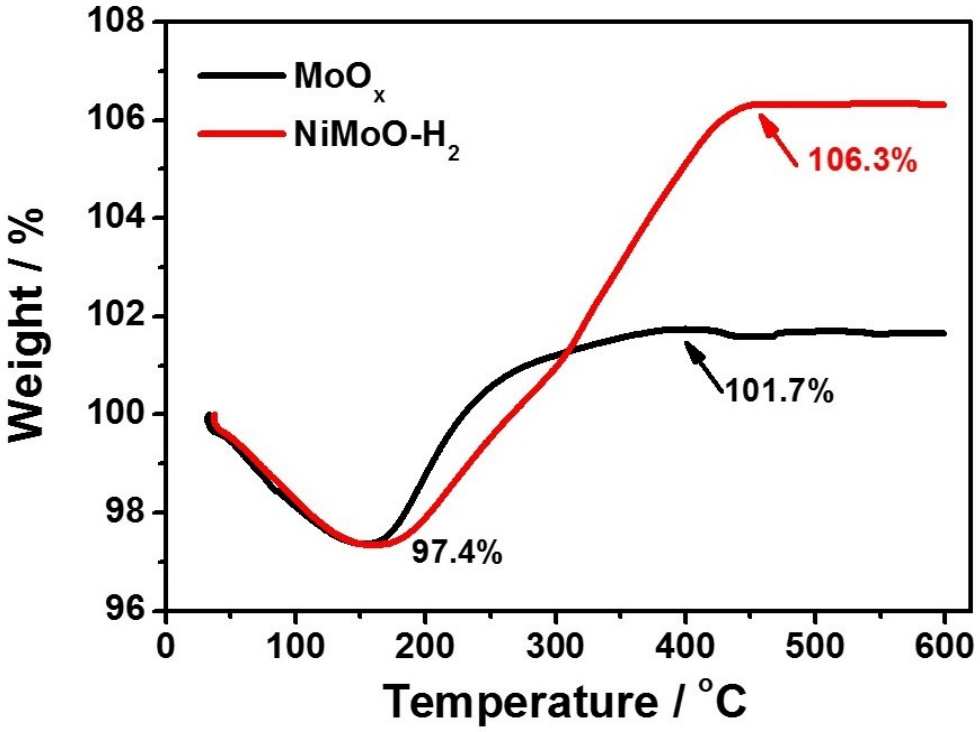

Fig. S5. TG analysis curves of MoO_x and NiMoO-H_2. The samples were treated in the TGA with a ramping rate of 10 ^oC min^{-1} in air atmosphere. The mass loss before 150 ^oC is due to the desorption of the adsorbed water and other small molecules. Then MoO_x and NiMoO-H_2 samples were oxidized in air, leading to the mass increase. Therefore, for MoO_x sample, the ratio of 97.4/101.7 corresponds to the molar mass ratio of MoO_x/MoO_3, resulting in $MoO_{2.62}$ for MoO_x. For the NiMoO-H_2 sample, the mass increase comes from the oxidation of both MoO_x and Ni. Due to the atom ratio of Ni/Mo is about unity from the ICP-AES result, we can estimate that the Ni/NiO atom ratio in NiMoO-H_2 is about 79/21.

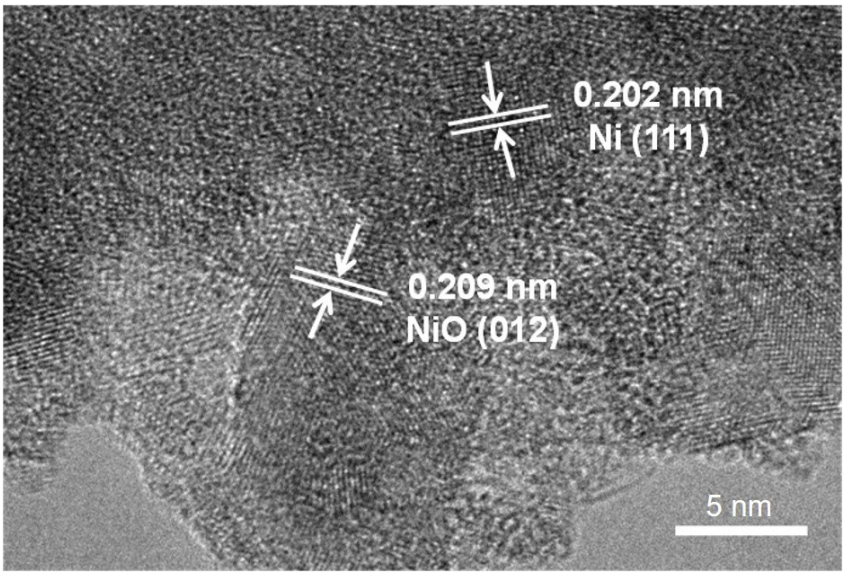

Fig. S6. HRTEM image of NiMoO-H_2.

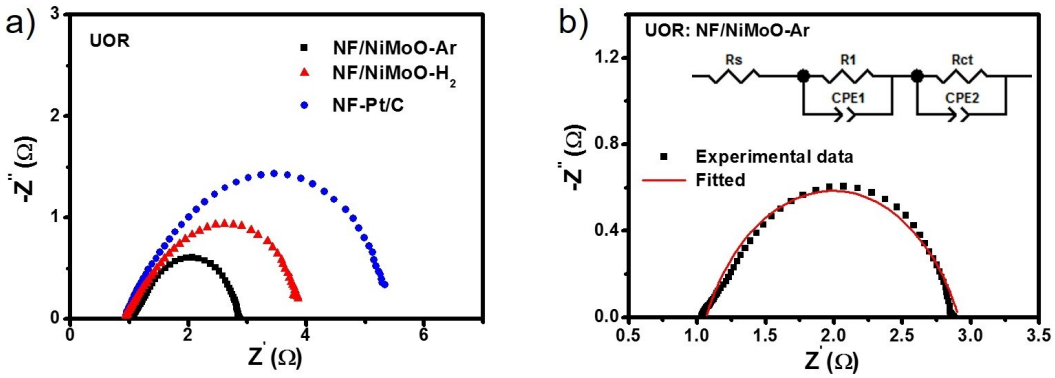

Fig. S7. a) Nyquist plots of different catalysts for UOR process at 1.38 V versus RHE. b) The corresponding fitting Nyquist plots for NF/NiMoO-Ar. Inset in (b) is the equivalent circuit. The equivalent circuit was consisted of a resistor (R_s) in series with two parallel combinations of a resistor (R_1 and R_{ct}) and a constant phase element (CPE_1 and CPE_2), in which R_s represents the uncompensated solution resistance, the time constant R_1-CPE_1 may relate to the interfacial resistance, and R_{ct}-CPE_2 reflects the charge-transfer resistance (R_{ct}).[1-3] The smallest R_{ct} for NF/NiMoO-Ar catalyst showed the fastest faradaic process and thus improves the UOR kinetics.

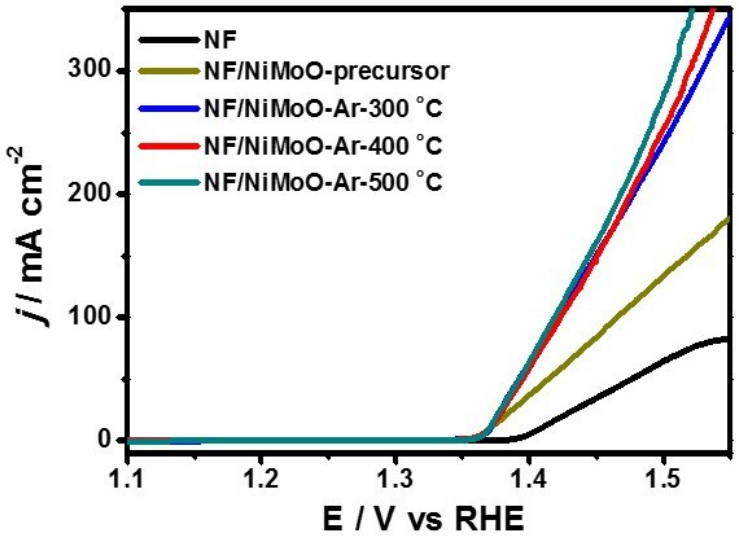

Fig. S8. UOR activity tests of NF/NiMoO-Ar catalysts treated at various annealing temperatures. NF/NiMoO-Ar treated at 300-500 ^{o}C showed the similar UOR activity, which is much better than the NF/NiMoO-precursor and bare NF samples. NF/NiMoO-Ar treated at 400 ^{o}C was chosen as the typical UOR catalyst for the better comparison with the best HER catalyst of NF/NiMoO-H_2, which was optimized at 400 ^{o}C.

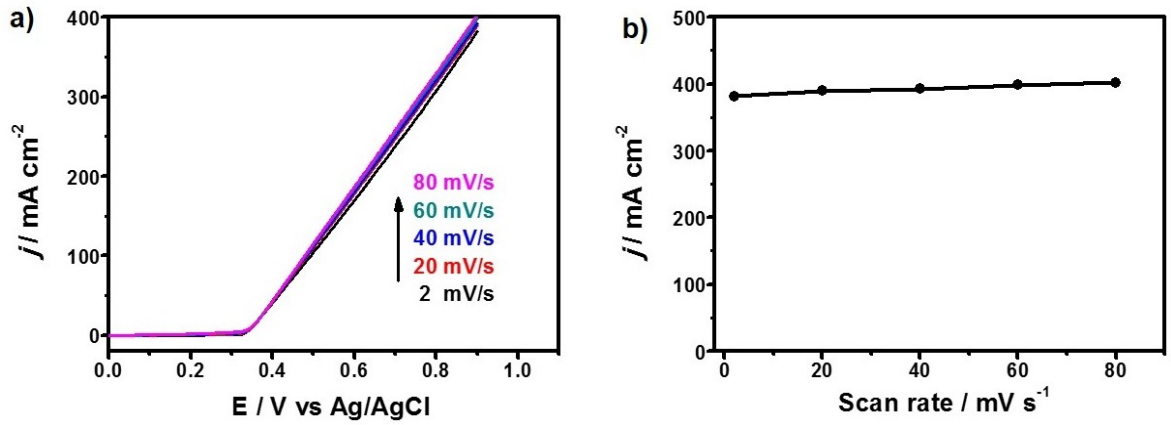

Fig. S9. a) UOR polarization plots of NF/NiMoO-Ar catalyst at different scan rates. b) The corresponding current densities at 0.9 V versus Ag/AgCl with different scan rates.

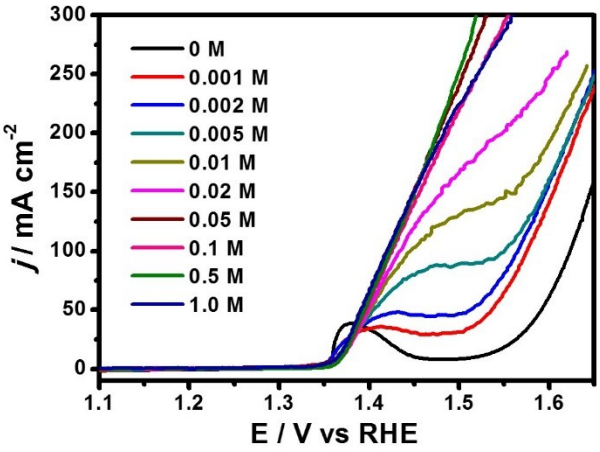

Fig. S10. UOR polarization curves of NF/NiMoO-Ar catalyst in 1 M KOH with various urea concentrations.

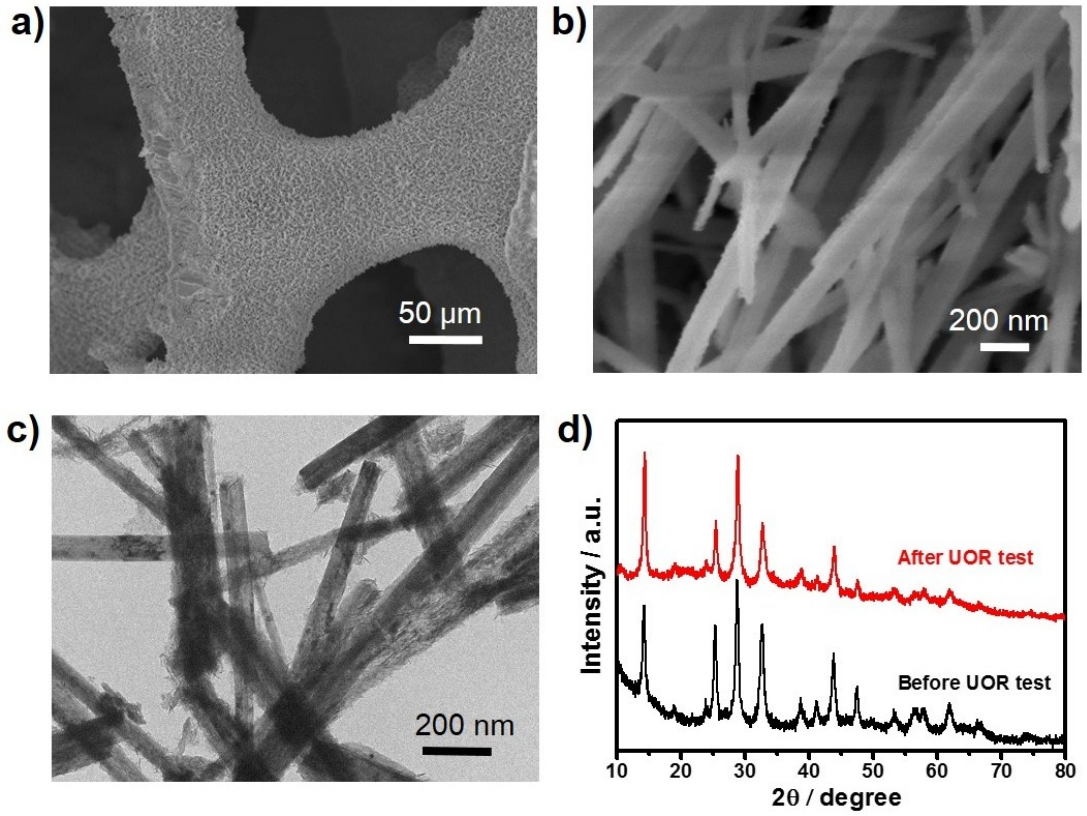

Fig. S11. a-c) SEM and TEM images of NiMoO-Ar catalyst after UOR cyclic tests. d) XRD patterns of NiMoO-Ar catalyst before and after UOR cyclic tests.

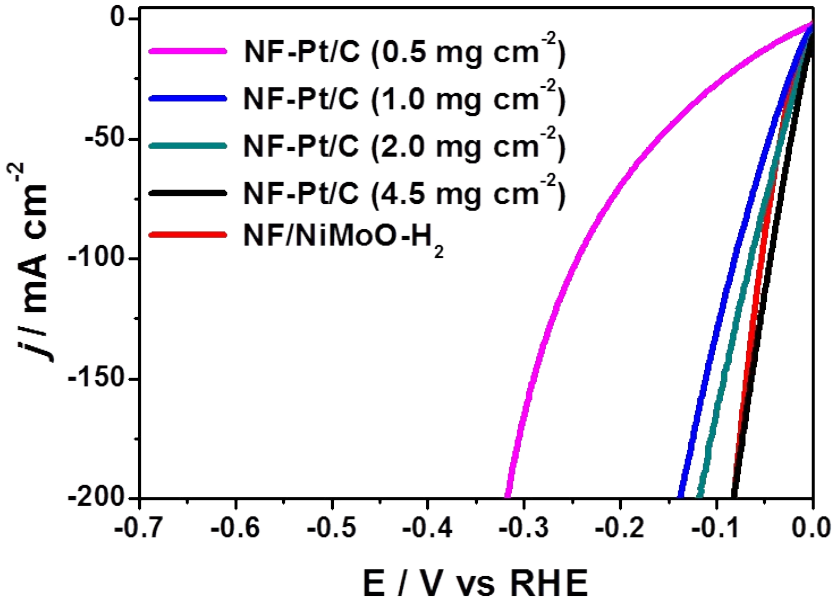

Fig. S12. HER polarization plots of commercial Pt/C (20 wt%) catalysts coated on Ni foam with different mass loadings.

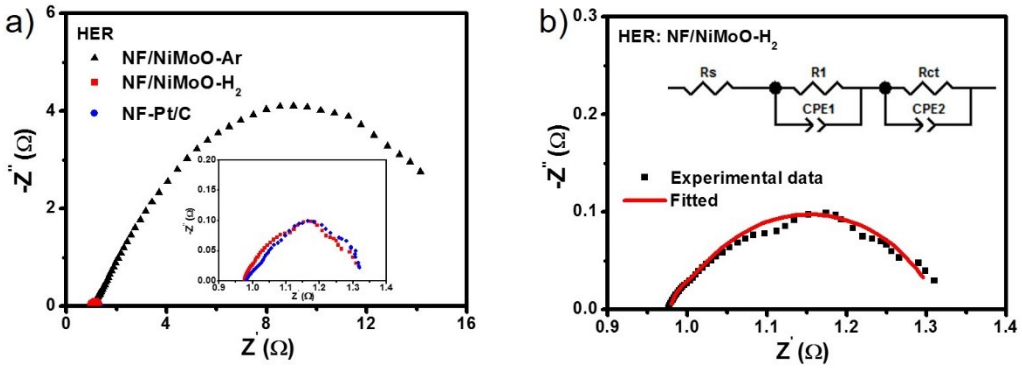

Fig. S13. a) Nyquist plots of different catalysts for HER process at -0.17 V versus RHE. Inset in (a) is the magnified Nyquist plots for NF/NiMoO-H_2 and NF-Pt/C catalysts. b) The corresponding fitting Nyquist plots for NF/NiMoO-H_2. Inset in (b) is the equivalent circuit. The equivalent circuit was consisted of a resistor (R_s) in series with two parallel combinations of a resistor (R_1 and R_{ct}) and a constant phase element (CPE_1 and CPE_2), in which R_s represents the uncompensated solution resistance, the time constant R_1-CPE_1 may relate to the interfacial resistance, and R_{ct}-CPE_2 reflects the charge-transfer resistance (R_{ct}).[1-3] The EIS analysis showed that NF/NiMoO-H_2 and NF-Pt/C catalysts had a similar HER kinetics process, enabling the excellent HER activity for NF/NiMoO-H_2.

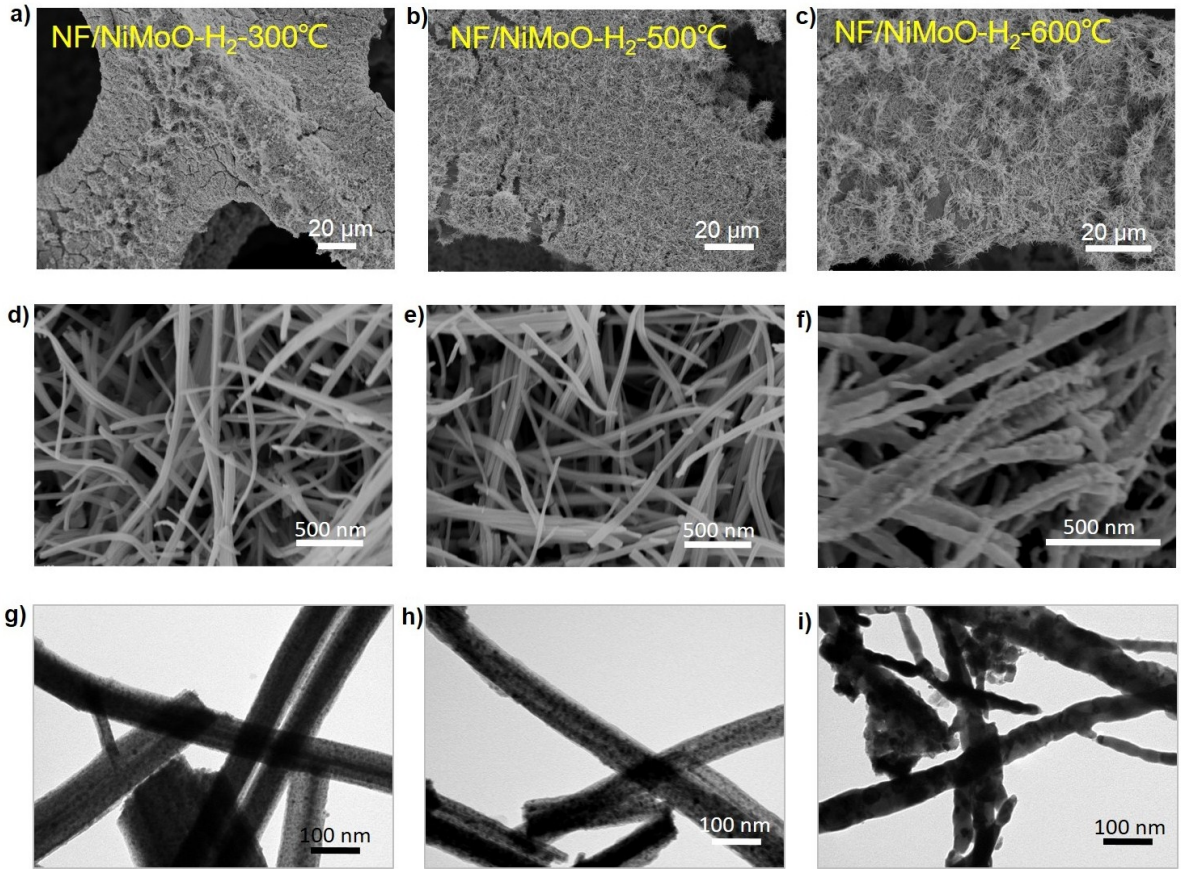

Fig. S14. Characterization of NF/NiMoO-H_2 treated at different temperatures. a,d,g) NF/NiMoO-H_2 treated at 300°C. b,e,h) NF/NiMoO-H_2 treated at 500 °C. c,f,i) NF/NiMoO-H_2 treated at 600 °C. a-c) SEM images of different samples. d-f) Enlarged SEM images of different samples. g-i) TEM images of different samples. The samples treated at 300-500 °C showed the similar morphology with nanoparticles decorated on the surface of nanorods. The 1D morphology of the sample treated at 600 °C was destroyed, which is consistent with the complete reduction of $NiMoO_4$ to Ni and Mo metals from the XRD result (Figure S15a).

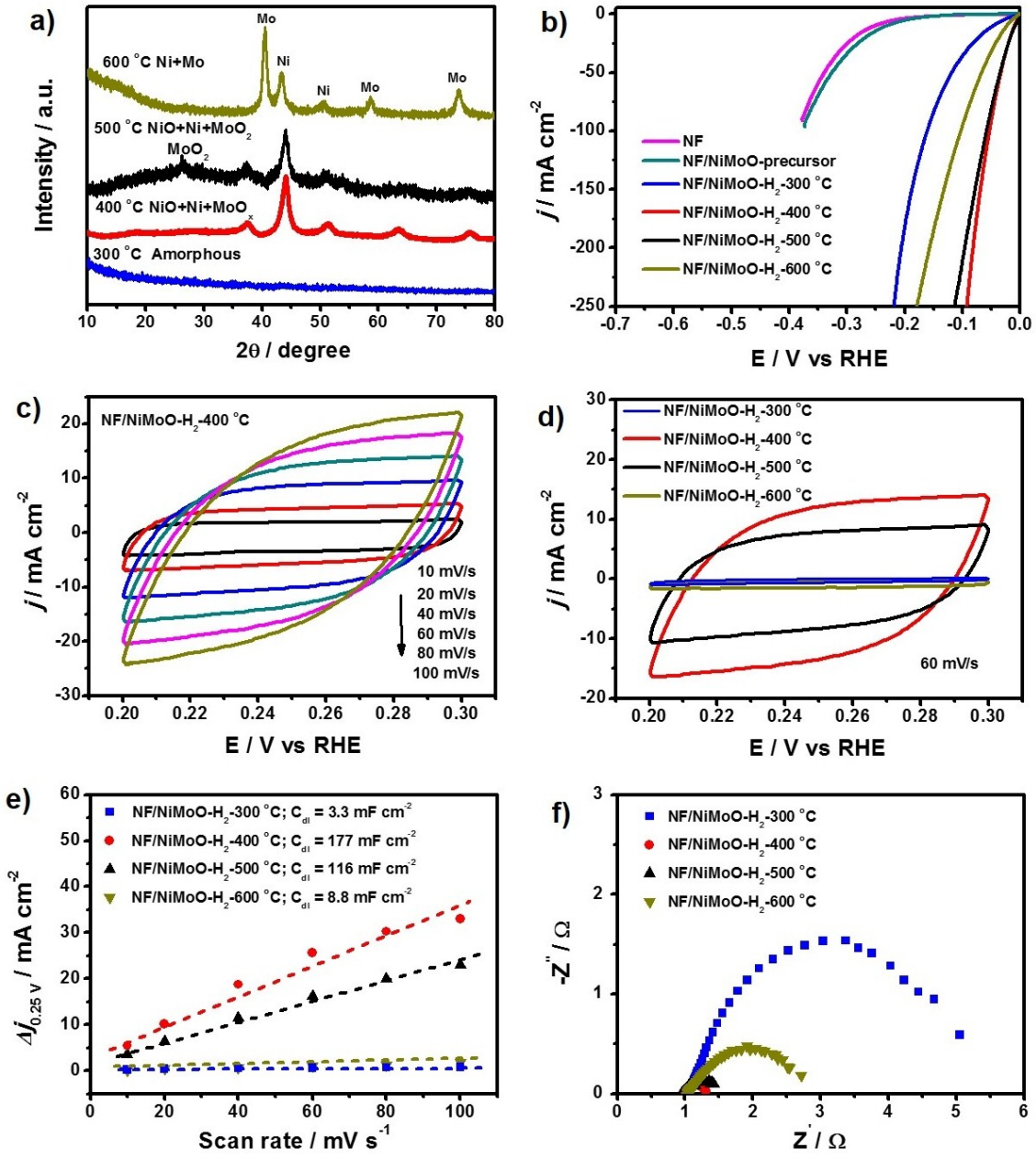

Fig. S15. HER activity tests of NF/NiMoO-H_2 treated at different temperatures. a) XRD patterns of different samples. b) HER polarization plots of different samples. c-e) Electrochemical surface area (ECSA) tests within a potential of 0.2-0.3 V versus RHE. c) CV curves of NF/NiMoO-H_2-400 °C at different scan rates. d) CV curves of different samples at a scan rate of 60 mV s^{-1}. e) The double-layer capacitance (C_{dl}) of different samples. f) EIS Nyquist plots of different samples at -0.17 V versus RHE.

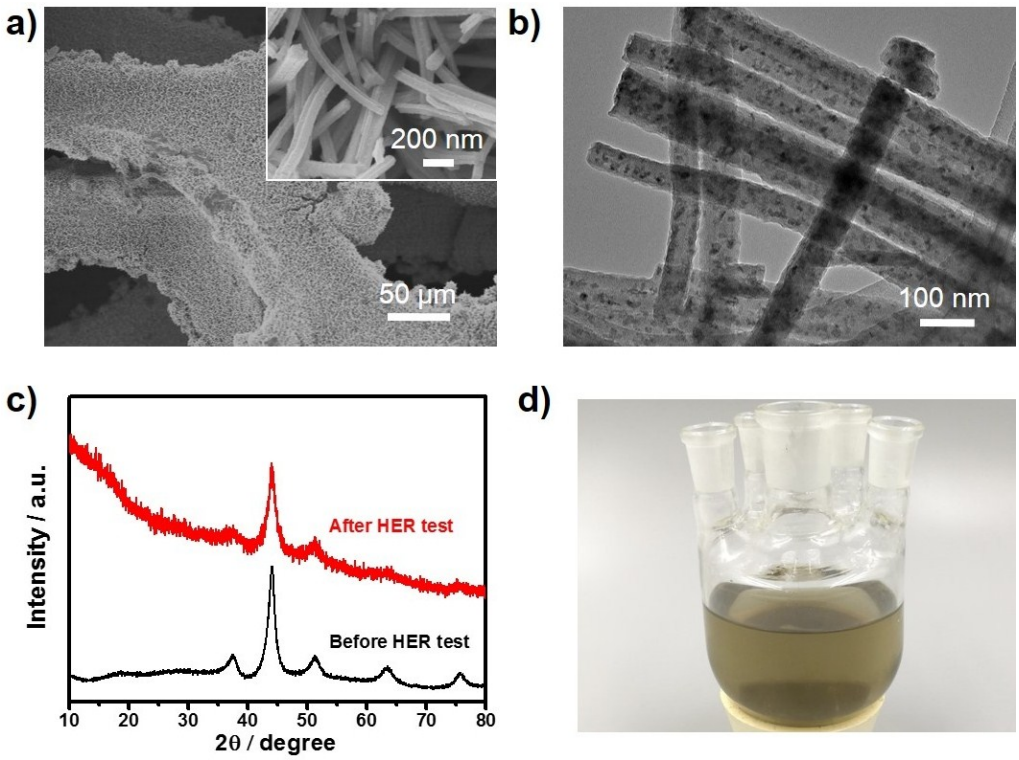

Fig. S16. a-b) SEM and TEM images of NiMoO-H_2 catalyst after HER cyclic tests. c) XRD patterns of NiMoO-H_2 catalyst before and after HER cyclic tests. d) The digital photo of electrolyte after the long-term HER test. We observed that the electrolyte became light brown color after long-term stability test, owing to some graphite exfoliated from the graphite counter electrode.

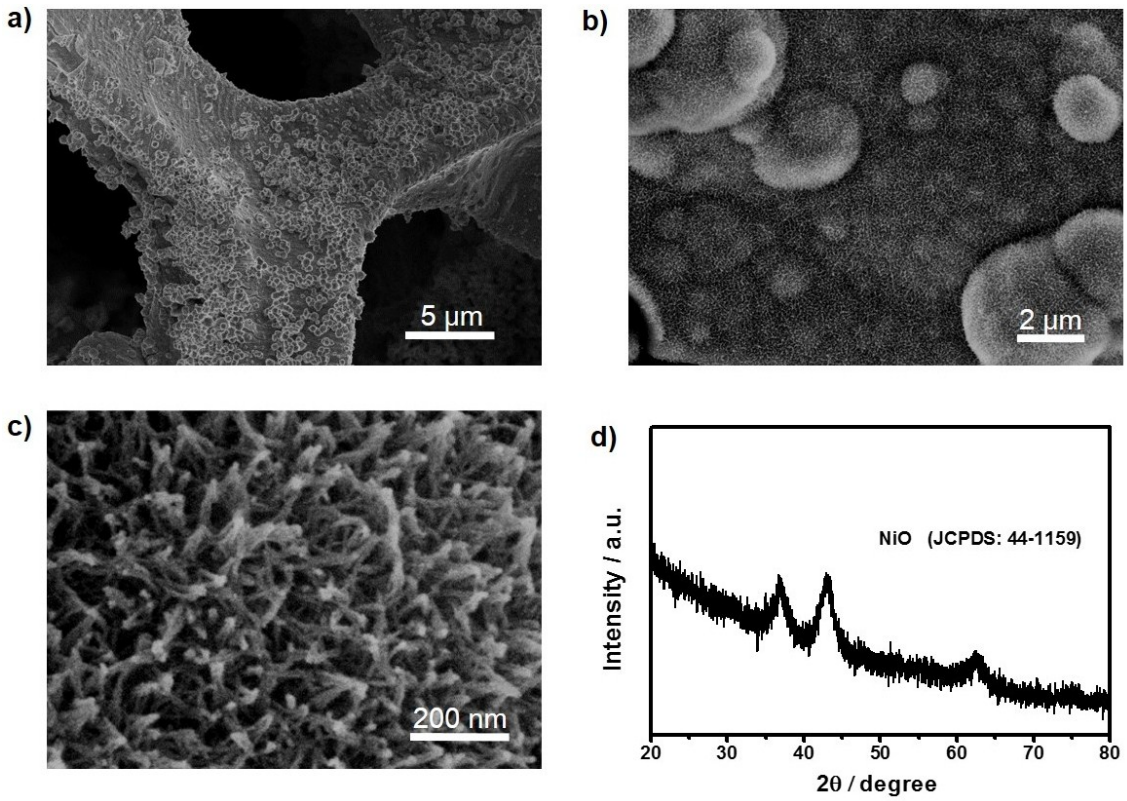

Fig. S17. Characterization of NF/NiO nanowire arrays without adding Mo source. a-c) Different magnifications of SEM images for NF/NiO nanowire arrays. d) XRD pattern of NiO powder. NiO nanowire arrays were grown on NF by a hydrothermal process and then annealing treatment.[4] $Ni(NO_3)_2 \cdot 6H_2O$ (1.5 mmol) and urea (6 mmol) were dissolved in 35 mL of H_2O. Then the mixed solution was transferred into a 50 mL Teflon-lined stainless steel autoclave and a piece of NF was immersed into the solution. After the autoclave kept at 120 ^oC for 8 h, the precursor of NF/$Ni(OH)_2$ can be obtained. Then NF/$Ni(OH)_2$ was annealed under Ar flow at 300 ^oC for 2 h to generate the NF/NiO sample. The mass loading of NiO nanowires on NF was optimized to about 5 mg cm^{-2}, which is close to the active mass loading of NF/NiMoO-Ar.

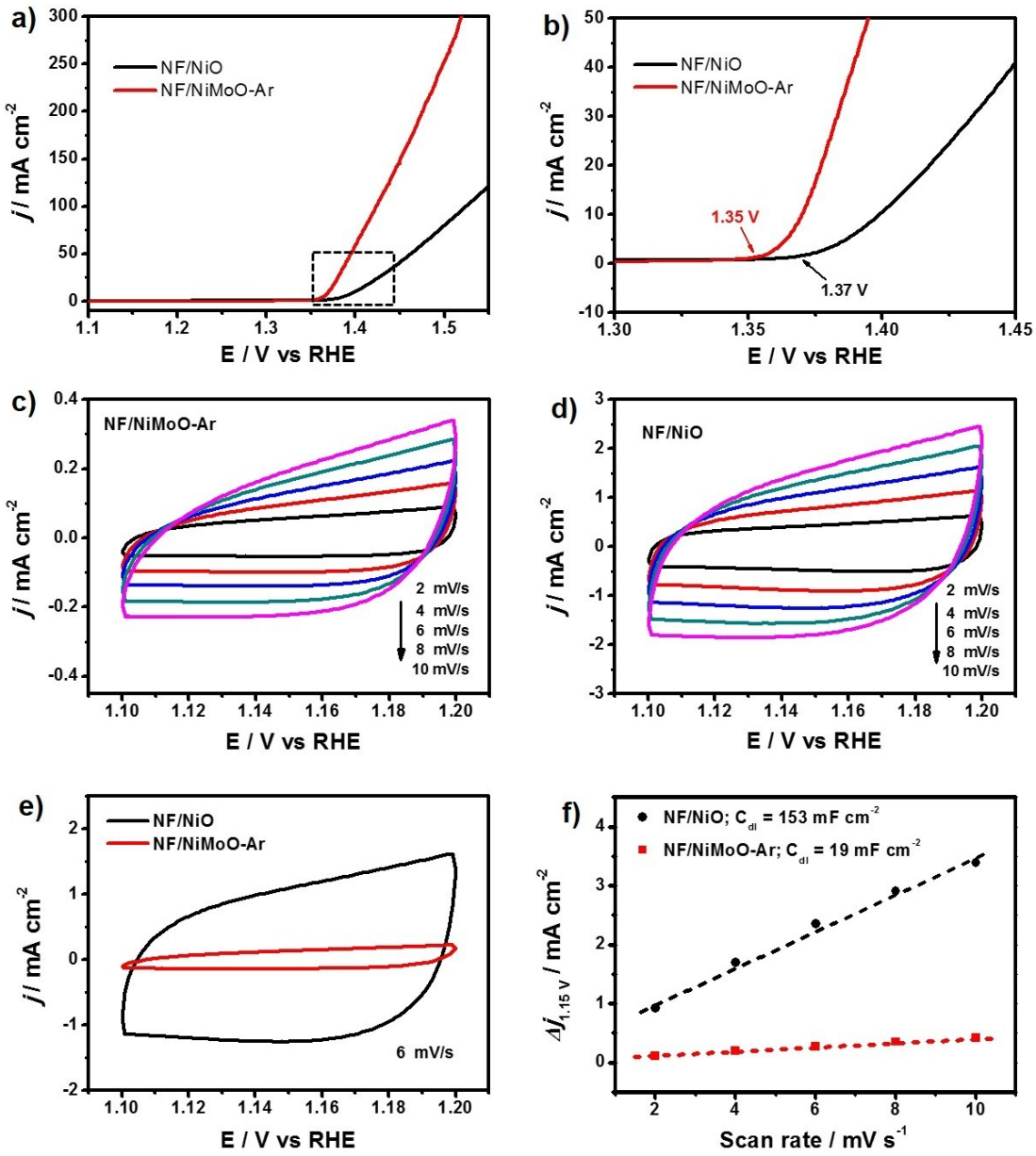

Fig. S18. UOR activity tests of NF/NiMoO-Ar and NF/NiO catalysts. a) UOR polarization plots of NF/NiMoO-Ar and NF/NiO catalysts. b) The magnified UOR polarization plots of (a). c-f) Electrochemical surface area (ECSA) tests within a potential of 1.1-1.2 V (versus RHE). c) CV curves of NF/NiMoO-Ar at different scan rates. d) CV curves of NF/NiO at different scan rates. e) The comparison of CV curves at a scan rate of 6 mV s^{-1}. f) The comparison of capacitive currents at different scan rates.

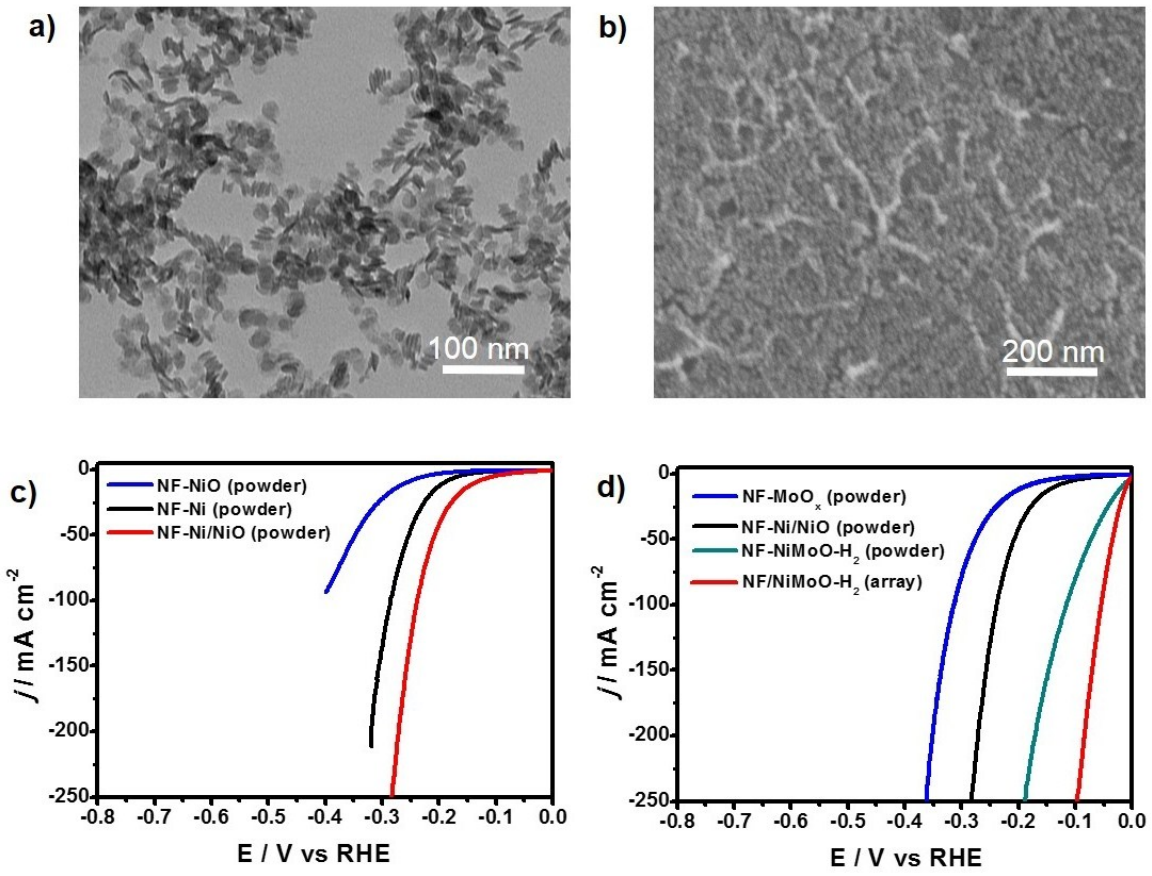

Fig. S19. HER activity tests. a) TEM image of $Ni(OH)_2$ nanoparticles as the precursor for the preparation of Ni/NiO. b) SEM image of NF-Ni/NiO (powder). c,d) HER polarization plots of different catalystscoating on NF with a mass loading of 4.5 mg cm^{-2}. We synthesized the Ni/NiO composite catalyst according to the recently reported work.[5,6] $Ni(OH)_2$ nanoparticles with a diameter of about 10 nm was used as the precursor. Then $Ni(OH)_2$ coated on NF was annealed under Ar atmosphere at 300°C with a low pressure by constantly pumping to generate NF-Ni/NiO (powder) catalyst. NF-Ni (powder) and NF-NiO (powder) were obtained by annealing NF-$Ni(OH)_2$ under H_2/Ar and Ar atmospheres at 300 °C, respectively.[5,6] The synergistic effect between Ni and NiO for the enhanced HER activity was confirmed from Fig. S19c, which is consistent with Dai's results.[5] MoO_x coated on NF was used as NF-MoO_x (powder) catalyst. NF-NiMoO-H_2 (powder) was obtained by coating NiMoO-precursor on NF and then treating under H_2/Ar at 400 °C. The HER activities of Ni/NiO and MoO_x were inferior to NiMoO-H_2 (Fig. S19d), showing that Ni, NiO, and MoO_x work together to boost the HER activity of NiMoO-H_2. In addition, the direct growth of NiMoO-H_2 nanorod arrays on NF can result in a better HER activity (Fig. S19d).

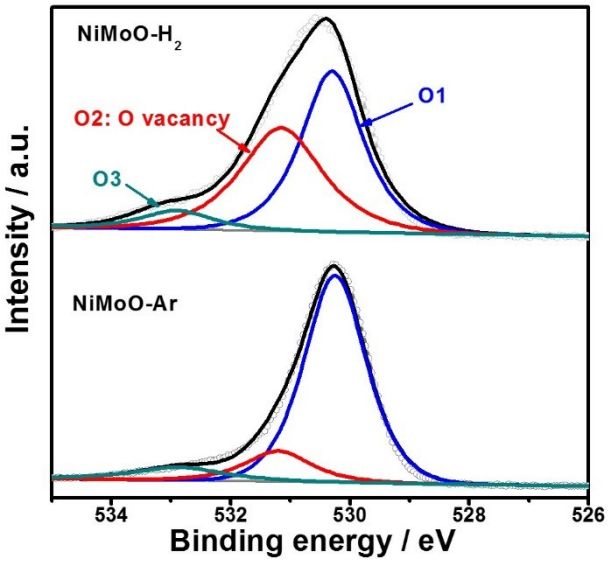

Fig. S20. High-resolution O 1s XPS spectra for NiMoO-H_2 and NiMoO-Ar.

The O 1s XPS spectra could be divided into three peaks, in which the O1 peak at 530.3 eV is associated with the lattice oxygen, the O2 peak at 531.2 eV is assigned to the oxygen vacancies, and the O3 peak at 532.9 eV is attributed to the hydroxy species of absorbed water molecules.[7-9] Obviously, NiMoO-H_2 had a much larger O2 peak area than NiMoO-Ar, indicating the generated oxygen vacancies by H_2 treatment. The excellent HER activity of NF/NiMoO-H_2 may be attributed to the oxygen vacancies.

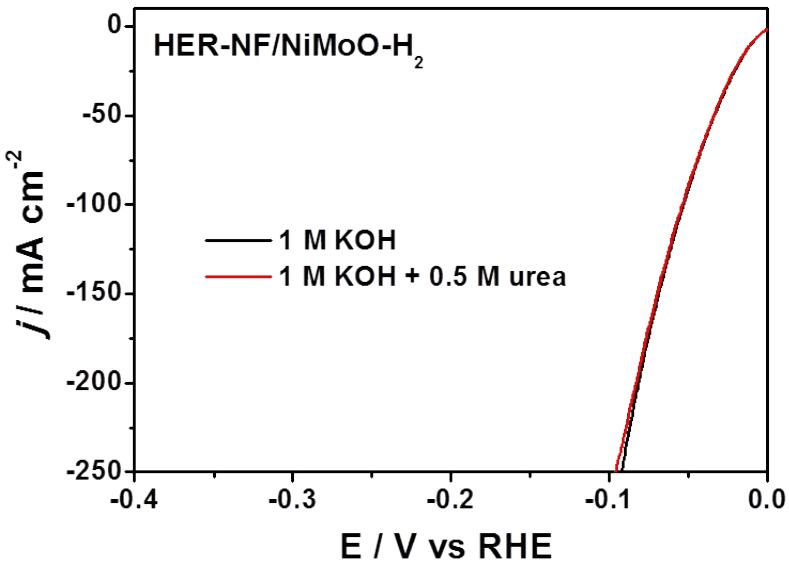

Fig. S21. HER polarization plots of NF/NiMoO-H_2 catalyst at a scan rate of 2 mV s^{-1} in 1 M KOH with or without 0.5 M urea electrolyte.

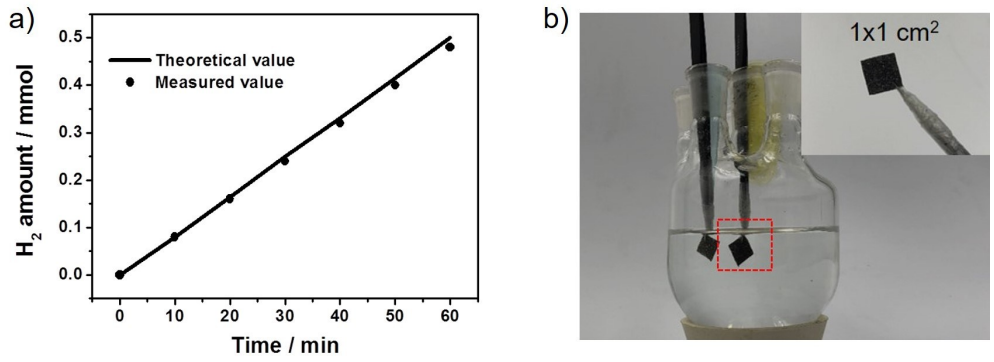

Fig. S22. a) H_2 amount was measured in a Hoffman apparatus for urea electrolysis. b) The digital photo of two-electrode urea electrolysis. Inset shows that tweezers's tip under the electrolyte was protected by the insulating parafilm and thus we can obtain the accurate current measurements.

We note that the electrode used in our study has a geometrical area of 1 cm^2, and therefore the current for the long-term stability test in Fig. 5d is about 0.1 A. Based on this, we can calculate that the total electric quantity is ~18,000 C during the continuous 50 h test, which leads to the mole number of transfer electron of ~0.186 mol. Considering the $6e^-$ transfer process of UOR ($CO(NH_2)_2 + 6OH^- \rightarrow N_2 + CO_2 + 5H_2O + 6e^-$), it equals the consumption of mere 0.031 mol urea, resulting in the urea concentration decreased from 0.5 M to 0.345 M after 50 h of continuous operation (200 mL electrolyte). We stress that such decrease of urea concentration has no effect on the UOR kinetics. As a matter of fact, our selected urea concentration of 0.5 M can sustain the electrolysis for more than 150 h, after that the urea concentration is reduced from 0.5 M to 0.02 M, and thus leads to inferior UOR kinetics. But at this point, we can provide additional urea into the electrolyte and enable the continuous electrolysis until the electrode degraded.

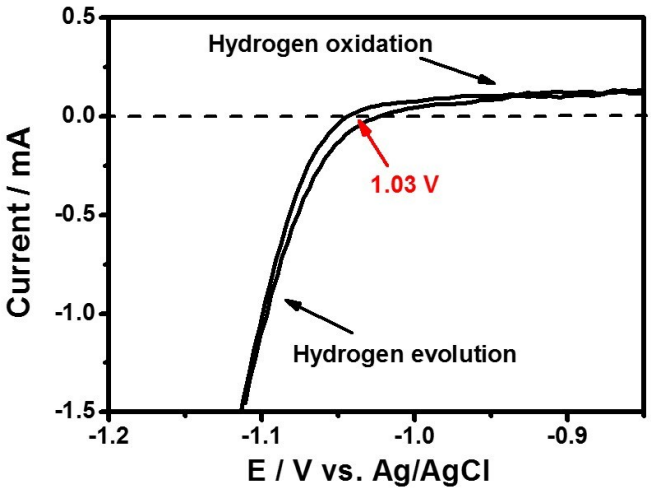

Fig. S23. The calibration curve of Ag/AgCl electrode in 1 M KOH.

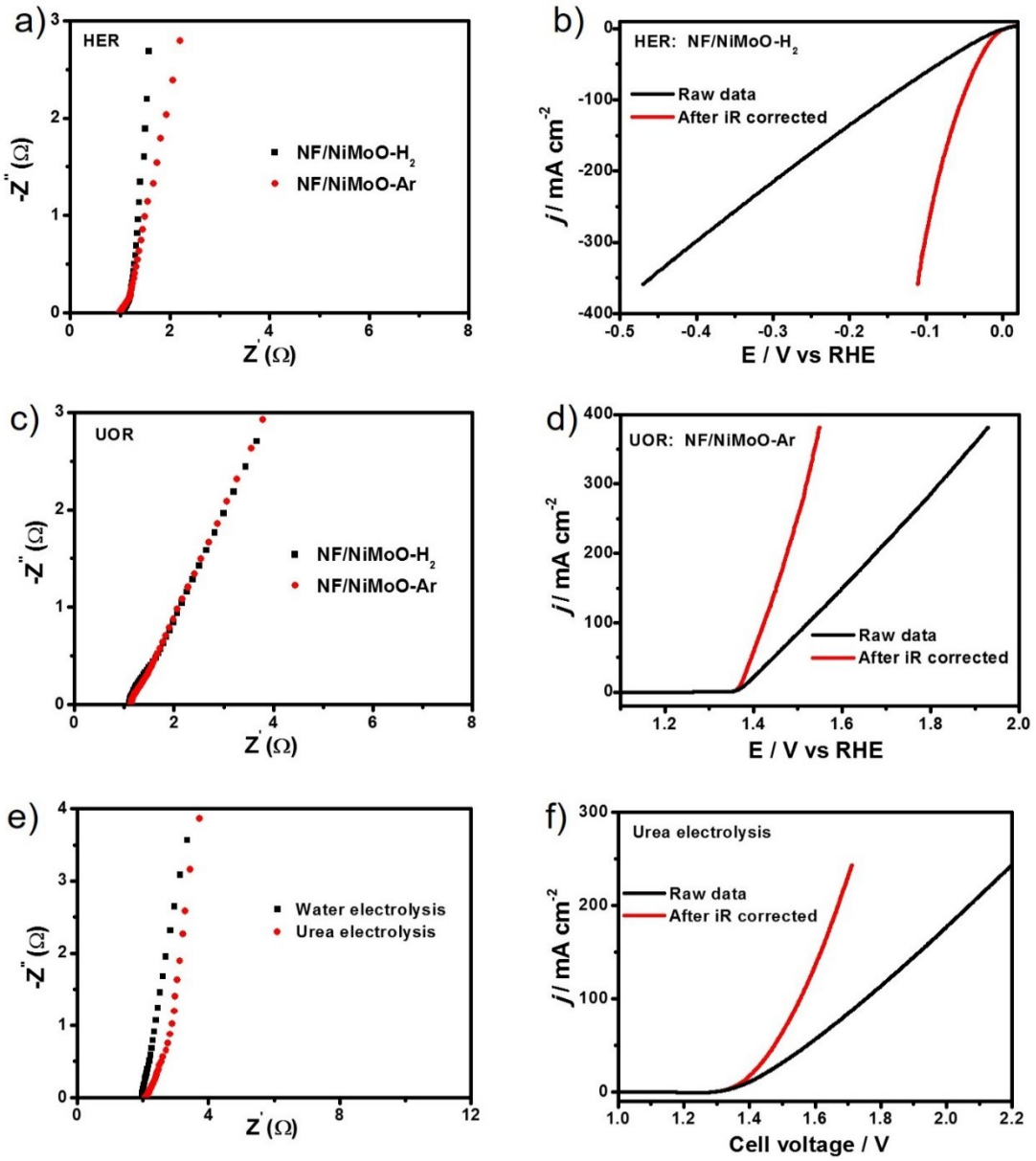

Fig. S24. a) Nyquist plots of different catalysts for HER process at open circuit potential. b) The HER polarization curves of NF/NiMoO-H_2 catalyst before and after iR compensation. c) Nyquist plots of different catalysts for UOR process at open circuit potential. d) The UOR polarization curves of NF/NiMoO-Ar catalyst before and after iR compensation. e) Nyquist plots of water electrolysis and urea electrolysis at open circuit potential. f) The polarization curves of urea electrolysis before and after iR compensation. The area of NF supported active materials is 1 cm^2.

Table S1. Comparison of the UOR performance of NF/NiMoO-Ar catalyst with other reported OER and UOR catalysts.

Catalyst	Anodic reaction	Tafel slope (mV dec^{-1})	j (mA cm^{-2})	Voltage (V) at the corresponding j	Reference
NF/NiFe-LDH	OER	N/A	10	1.47	10
NF/Ni_3S_2	OER	N/A	10	1.49	11
Cu foil/Co_3O_4-C	OER	70	10	1.52	12
NF/Ni@Mo_2C-PC	OER	150	10	1.53	13
CC/CoO	OER	44	10	1.56	14
Au foil/CoP/PO_4	OER	65	30	1.56	15
$Ni(OH)_2$	UOR	N/A	10	~1.42	16
$Ni(OH)_2$-graphene	UOR	N/A	10	~1.43	17
NiCo alloy	UOR	N/A	10	~1.50	18
NF-Pt/C	UOR	105	10	1.48	19
NF/MnO_2	UOR	75	10	1.33	19
			100	1.45	
NF/NiMoO-Ar	UOR	19	10	1.37	This work
			100	1.42	

Table S2. Comparison of the HER performance for NF/NiMoO-H_2 catalyst with other reported 3D HER catalysts in 1 M KOH electrolyte.

Catalyst	Mass loading (mg cm^{-2})	Tafel slope (mV dec^{-1})	j (mA cm^{-2})	η_j (mV)	Reference
NF/NiO@Ni-CNT	8	51	100	95	5
NF/NiO@Ni@Cr_2O_3	8	N/A	100	150[1]	6
NF/NiFe-LDH	N/A	N/A	10	210	10
NF/Ni_3S_2	1.6	N/A	10	223	11
NF/$MoNi_4$-MoO_2	43.4	30	10	15	20
NF/$MoNi_4$-MoO_{3-x}	8.7	36	10	17	21
NF/MoO_2	4.5	66	10	55	22
NF/NiS_x	142.2	99	10	60	23
NF/$Co(OH)_2$@PANI	0.74	91.6	10	88	24
CFP/$NiFeO_x$[2]	1.6	150.2	10	88	25
NF/NiSe	2.8	120	10	96	26
CFP/NiP_x[2]	25.8	58.8	10	117	27
NF/CoO_x@CN	2.1	N/A	20	134	28
CC/CoP[3]	0.92	129	10	209	29
NF-Pt/C	4.5	38	10 100 300	2 44 118	This work
NF/NiMoO-H_2	4.5	43	10 100 300	11 53 102	This work

[1] This value is reported without iR compensation.
[2-3] CFP and CC were denoted as the 3D conductive carbon fiber paper and carbon cloth, respectively.

Table S3. Comparison of the activity of our urea electrolyser with other reported electrolysers.

Catalyst	Reaction	*j* (mA/cm^2)	Voltage (V) at the corresponding j	Reference
CFP/$NiFeO_x$	Water electrolysis	10	~1.51	25
NF/MoO_2	Water electrolysis	10	1.53	30
NF/NiSe	Water electrolysis	10	1.63	26
NF/Ni@Mo_2C-PC	Water electrolysis	10	1.66	13
NF/NiFe LDH	Water electrolysis	10	1.70	10
NF/Ni_3S_2	Water electrolysis	13	1.76	11
NF/Ni_2P	HMF oxidation reaction with HER[1]	10	1.44	31
NF/Ni_3S_2	HMF oxidation reaction with HER[1]	10	1.46	32
NF/MnO2 // NF/CoP_x	Urea electrolysis	10 30	1.41 1.80	19
NF-Pt/C	Urea electrolysis	10	1.68	19
NF-Pt/C // NF-IrO_2	Urea electrolysis	10	1.72	19
NF/NiMoO-Ar // NF/NiMoO-H_2	Urea electrolysis	10 100	1.38 1.55	This work

[1] The anodic reaction is the oxidation of 5-hydroxymethylfurfural (HMF) to 2,5-furandicarboxylic acid (FDCA).

References

1. X. Wang, Y. V. Kolen'ko, X.-Q. Bao, K. Kovnir and L. Liu, *Angew. Chem. Int. Ed.*, 2015, **54**, 8188-8192.
2. L. Liao, S. Wang, J. Xiao, X. Bian, Y. Zhang, M. D. Scanlon, X. Hu, Y. Tang, B. Liu and H. H. Girault, *Energy Environ. Sci.*, 2014, **7**, 387-392.
3. L. Feng, H. Vrubel, M. Bensimon and X. Hu, *Phys. Chem. Chem. Phys.*, 2014, **16**, 5917-5921.
4. Z. Lu, Z. Chang, J. Liu and X. Sun, *Nano Res.*, 2011, **4**, 658-665.
5. M. Gong, W. Zhou, M.-C. Tsai, J. Zhou, M. Guan, M.-C. Lin, B. Zhang, Y. Hu, D.-Y. Wang, J. Yang, S. J. Pennycook, B.-J. Hwang and H. Dai, *Nat. Commun.*, 2014, **5**, 4695.
6. M. Gong, W. Zhou, M. J. Kenney, R. Kapusta, S. Cowley, Y. Wu, B. Lu, M.-C. Lin, D.-Y. Wang, J. Yang, B.-J. Hwang and H. Dai, *Angew. Chem. Int. Ed.*, 2015, **54**, 11989-11993.
7. K. K. Banger, Y. Yamashita, K. Mori, R. L. Peterson, T. Leedham, J. Rickard and H. Sirringhaus, *Nat. Mater.*, 2010, **10**, 45.
8. S. Gao, Z. Sun, W. Liu, X. Jiao, X. Zu, Q. Hu, Y. Sun, T. Yao, W. Zhang, S. Wei and Y. Xie, *Nat. Commun.*, 2017, **8**, 14503.
9. J. Yin, Y. Li, F. Lv, M. Lu, K. Sun, W. Wang, L. Wang, F. Cheng, Y. Li, P. Xi and S. Guo, *Adv. Mater.*, 2017, **29**, 1704681.
10. J. Luo, J.-H. Im, M. T. Mayer, M. Schreier, M. K. Nazeeruddin, N.-G. Park, S. D. Tilley, H. J. Fan and M. Grätzel, *Science*, 2014, **345**, 1593-1596.
11. L.-L. Feng, G. Yu, Y. Wu, G.-D. Li, H. Li, Y. Sun, T. Asefa, W. Chen and X. Zou, *J. Am. Chem. Soc.* , 2015, **137**, 14023-14026.
12. T. Y. Ma, S. Dai, M. Jaroniec and S. Z. Qiao, *J. Am. Chem. Soc.*, 2014, **136**, 13925-13931.
13. Z.-Y. Yu, Y. Duan, M.-R. Gao, C.-C. Lang, Y.-R. Zheng and S.-H. Yu, *Chem. Sci.*, 2017, **8**, 968-973.
14. T. Ling, D.-Y. Yan, Y. Jiao, H. Wang, Y. Zheng, X. Zheng, J. Mao, X.-W. Du, Z. Hu, M. Jaroniec and S.-Z. Qiao, *Nat. Commun.*, 2016, **7**, 12876.
15. Y. Yang, H. Fei, G. Ruan and J. M. Tour, *Adv. Mater.*, 2015, **27**, 3175-3180.
16. X. Zhu, X. Dou, J. Dai, X. An, Y. Guo, L. Zhang, S. Tao, J. Zhao, W. Chu, X. C. Zeng, C. Wu and Y. Xie, *Angew. Chem. Int. Ed.*, 2016, **55**, 12465-12469.
17. D. Wang, W. Yan, S. H. Vijapur and G. G. Botte, *Electrochem. Acta*, 2013, **89**, 732-736.
18. W. Xu, H. Zhang, G. Li and Z. Wu, *Sci. Rep.*, 2014, **4**, 5863.
19. S. Chen, J. Duan, A. Vasileff and S. Z. Qiao, *Angew. Chem. Int. Ed*, 2016, **55**, 3804-3808.
20. J. Zhang, T. Wang, P. Liu, Z. Liao, S. Liu, X. Zhuang, M. Chen, E. Zschech and X. Feng, *Nat. Commun.*, 2017, **8**, 15437.
21. Y.-Y. Chen, Y. Zhang, X. Zhang, T. Tang, H. Luo, S. Niu, Z.-H. Dai, L.-J. Wan and J.-S. Hu, *Adv. Mater.*, 2017, **29**, 1703311.
22. Y. Jin and P. K. Shen, *J. Mater. Chem. A*, 2015, **3**, 20080-20085.
23. B. You and Y. Sun, *Adv. Energy Mater.*, 2016, **6**, 1502333.
24. J.-X. Feng, L.-X. Ding, S.-H. Ye, X.-J. He, H. Xu, Y.-X. Tong and G.-R. Li, *Adv. Mater.*, 2015, **27**, 7051-7057.
25. H. Wang, H.-W. Lee, Y. Deng, Z. Lu, P.-C. Hsu, Y. Liu, D. Lin and Y. Cui, *Nat. Commun.*, 2015, **6**, 7261.

26. C. Tang, N. Cheng, Z. Pu, W. Xing and X. Sun, *Angew. Chem. Int. Ed.*, 2015, **54**, 9351-9355.
27. X. Wang, W. Li, D. Xiong, D. Y. Petrovykh and L. Liu, *Adv. Funct. Mater.*, 2016, **26**, 4067-4077.
28. H. Jin, J. Wang, D. Su, Z. Wei, Z. Pang and Y. Wang, *J. Am. Chem. Soc.*, 2015, **137**, 2688-2694.
29. J. Tian, Q. Liu, A. M. Asiri and X. Sun, *J. Am. Chem. Soc.*, 2014, **136**, 7587-7590.
30. Y. Jin, H. Wang, J. Li, X. Yue, Y. Han, P. K. Shen and Y. Cui, *Adv. Mater.*, 2016, **28**, 3785-3790.
31. B. You, N. Jiang, X. Liu and Y. Sun, *Angew. Chem. Int. Ed.*, 2016, **55**, 9913-9917.
32. B. You, X. Liu, N. Jiang and Y. Sun, *J. Am. Chem. Soc.*, 2016, **138**, 13639-13646.